On the use of PN Ranging with High-rate Spectrally-efficient Modulations in Satellite Payload Telemetry Links

On the use of PN Ranging with High-rate Spectrally-efficient Modulations in Satellite Payload Telemetry Links

Barbara Ripani, Student Member, IEEE
Politecnico di Torino, Torino, Italy

Andrea Modenini
European Space Agency (ESA-ESTEC), Noordwijk, Netherlands

Guido Montorsi, Fellow, IEEE
Politecnico di Torino, Torino, Italy

***Abstract*—Pseudo Noise (PN) ranging ([1]–[3]) is a ranging technique that has been recently introduced in near-Earth space research (SR) missions. For these, at the state-of-the-art, the PN ranging signal is combined with a high-rate telemetry stream binary modulated in phase. The coupling of the two, together with the 10 MHz bandwidth constraint imposed for this class of missions ([4], [5]), translates into a data rate bound of approximately 10 Mbps. The purpose of this article is to prove the feasibility of overcoming the current data rate limitation by defining a communication architecture that foresees the coupling of the PN ranging signal with a high-order modulated telemetry stream.**

To achieve the goal, we study the feasibility of pairing the PN ranging with filtered high-order modulations that are standardized for satellite payload telemetry links and investigate the simultaneous demodulation of the telemetry stream while tracking the ranging sequence. Accordingly, we design a receiver scheme capable of performing a closed-loop parallel cancellation of the ranging and the telemetry signal reciprocally. From our analysis, we find that the non-constant envelope property, characterizing the considered modulation set, causes an additional jitter on the PN ranging timing estimation that, on the other hand, can be controlled and reduced by proper sizing the receiver loop bandwidth without limiting the timing synchronization dynamic. Our study proves the use of filtered high-order modulations combined with PN ranging to outperform the state-of-the-art in terms of spectral efficiency and achievable data rate while having comparable ranging performance.

Manuscript submitted 20 October, 2021.

Barbara Ripani and Guido Montorsi are with Politecnico di Torino, Corso Duca degli Abruzzi 24, I-10129 Torino, Italy (e-mail: barbara.ripani@studenti.polito.it; guido.montorsi@polito.it). Andrea Modenini is with the European Space Agency (ESA-ESTEC), Keplerlaan 1, 2201AZ Noordwijk, The Netherlands (e-mail: andrea.modenini@esa.int).

The view expressed herein can in no way be taken to reflect the official opinion of the European Space Agency. The paper was presented in part at the International Conference on Space Operations (SpaceOps), held virtually in May 2021.

***Index Terms*—Telemetry, communication system performance, phase shift keying, radio position measurement, modulation.**

I. INTRODUCTION

EVERY space mission relies upon the knowledge of the spacecraft's position and velocity. Tracking a satellite's orbit, along with its deviation from the estimated flight path, is known as orbit determination and depends on several types of measurements tailored for each space mission. Some examples are Global Navigation Satellite System (GNSS) data, distance and velocity measurements based on ranging techniques and tracking data (including antenna angles) through an auto-track mode of the ground station antenna [6], [7].

Ranging techniques rely on a signal transmitted from the ground station to the satellite, and back to Earth. Then, a measure of the distance between the satellite and the ground station is retrieved from the round trip light time of the ranging signal. Over the years, space agencies developed different ranging systems, like the NASA sequential ranging and the ESA code ranging [8], [9]. Lately, to meet the demanded positioning accuracy while granting the cross-support among space agencies, the Consultative Committee for Space Data Systems (CCSDS) standardized the PN ranging [1], [10]. This last is a state-of-the-art positioning technique that permits the on-board ranging regeneration, thus enhancing the signal-to-noise ratio (SNR) received on Earth. The standard, which envisions the simultaneous transmission of PN ranging with high-rate Gaussian minimum shift keying (GMSK)-modulated telemetry, ensures determining the spacecraft position while receiving the high-rate telemetry stream.

Future SR missions (e.g., JUICE [11]) will widely adopt PN ranging combined with GMSK: this was already implemented in the ESA missions BepiColombo and Solar Orbiter, and demonstrated an accuracy as high as a few centimeters during its validation [3], [12]. On the other hand, Telemetry Tracking and Command (TT&C) and payload data transmission (PDT) for near-Earth SR missions usually take place in the X-Band (8.4-8.45 GHz). This frequency allocation constraints the occupied bandwidth to 10 MHz [4]. Thus, when using GMSK, SR missions are limited to a data rate of about 10 Mbps, penalizing the payload data generation. Therefore, to overcome the current data rate bound, this class of missions requires efficient use of the available X-Band bandwidth. For this reason, one must resort to high-order modulation schemes. Their compatibility with PN ranging was investigated only with multi-h continuous phase modulations (CPM) in [21]. However, this study focuses on optimizing the ranging shaping pulse for improving accuracy. Additionally, multi-h CPMs do not maximize spectral efficiency, and TT&C/PDT standards do not foresee them.

In this paper, differently, we study the coupling of PN ranging with filtered (amplitude) phase-shift keying

(PSK/APSK) signals by taking as reference the CCSDS standard 131.2 ([13], [14]). Namely, we define a receiver scheme that can simultaneously demodulate the PSK/APSK stream (with modulation orders as high as 64) and track the PN ranging sequence. This is done by performing a parallel closed-loop cancellation of the PN ranging sequence over the telemetry symbols and vice-versa. To evaluate the performance of the designed system, both under linear and nonlinear conditions, we assess the bit error rate (BER) and the ranging timing jitter. This last reveals the presence of a noise floor due to the non-constant envelope of PSK/APSK modulations. By modeling this phenomenon, we derive a closed-form approximation for the ranging jitter.

In this work, we find the performance of the proposed scheme to be comparable to the classical GMSK approach while enabling much higher data rates, thus paving the way towards the next generation of near-Earth SR missions with more ambitious scientific objectives.

The remainder of this paper is organized as follows: Section II outlines the mathematical model that describes the proposed communication architecture inclusive of the transmission system and channel model. Section III mainly focuses on the description of the implemented receiver system. Then, Section IV analyzes and mathematically describes the impact on the timing jitter when combining non-constant envelope modulations with the PN ranging signal. Section V first shows the results coming from computer simulations, then presents examples of application to two space missions: the already deployed GAIA satellite and the possible future mission GAIA-NIR. Finally, Section VI draws conclusions.

II. System Model

This section describes the system model adopted by this paper, namely, the transmission system and the channel model.

A. Transmission System

We consider the transmission system described by the block diagram reported in Figure 1. The complex baseband modulated telemetry signal, with unitary power, is defined as

$$x_{\mathrm{TM}}(t) = \sum_k a_k p(t - kT)\,, \tag{1}$$

where $p(t)$ is the square root raised cosine (SRRC) shaping pulse, and $\{a_k\}$ the sequence of telemetry symbols, each transmitted at symbol time kT, and belonging to a complex PSK/APSK constellation. Instead, the phase-modulated ranging signal $r_{\mathrm{RG}}(t)$ is defined as $r_{\mathrm{RG}}(t) = e^{j\Phi_{\mathrm{RG}}(t)}$. Its phase can be expressed as

$$\Phi_{\mathrm{RG}}(t) = m_{\mathrm{RG}} \sum_k c_k h(t - kT_c)\,, \tag{2}$$

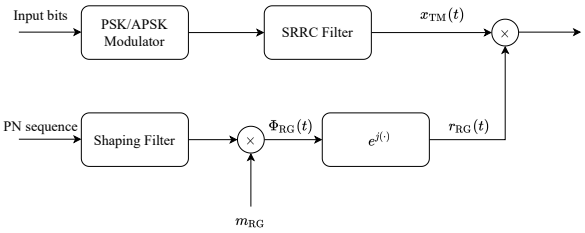

Fig. 1. Transmitter block diagram.

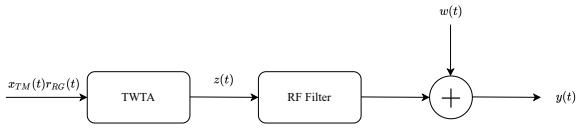

Fig. 2. Nonlinear Channel Model Block Diagram.

where m_{RG} is the ranging modulation index, $h(t)$ a sinusoidal chip shaping pulse [1] that reads

$$h(t) = \sin\left(\frac{\pi t}{T_c}\right)\,, \quad t \in [0, T_c]\,, \tag{3}$$

and $c_k \in \{\pm 1\}$ the ranging code chip transmitted at time kT_c and generated according to a balanced Tausworthe scheme [1]. Note that, in line with CCSDS recommendation 2.4.22A [15] and considering that we target high bit rates, we imposed $T_c \neq nT$, with $n \in \mathbb{Z}^+$, and consider $T_c > T$.

B. Channel Model

We consider linear and nonlinear channel models. We adopt the additive white Gaussian noise (AWGN) channel for the linear case. The received signal reads

$$y(t) = x_{\mathrm{TM}}(t) \cdot r_{\mathrm{RG}}(t - \tau_{\mathrm{RG}}) + w(t)\,, \tag{4}$$

where $w(t)$ is white Gaussian noise with spectral density equal to N_0, and $\tau_{\mathrm{RG}} \in [-\frac{T_c}{2}, \frac{T_c}{2})$ is an arbitrary ranging timing delay. Differently, the nonlinear channel considers signal distortions introduced by a power amplifier. In this paper, we use the nonlinear channel model described by the block diagram of Figure 2. It is composed of a traveling wave tube amplifier (TWTA) followed by an RF filter which compensates for the spectral regrowth. In Figure 2, the signal output from the TWTA is modeled as

$$z(t) = f_{AM}(\cdot)e^{j\angle\cdot + f_{PM}(\cdot)}\,, \tag{5}$$

being $f_{AM}(\cdot)$ and $f_{PM}(\cdot)$ the normalized AM/AM and AM/PM characteristics shown in Figure 3 and 4, respectively. Instead, the RF filter is implemented as an elliptic filter, having a passband of about 12.5 MHz.

III. Receiver for PSK/APSK-modulated signals and PN Ranging

In this section, we provide the mathematical details of the receiver scheme. We consider a modified version of

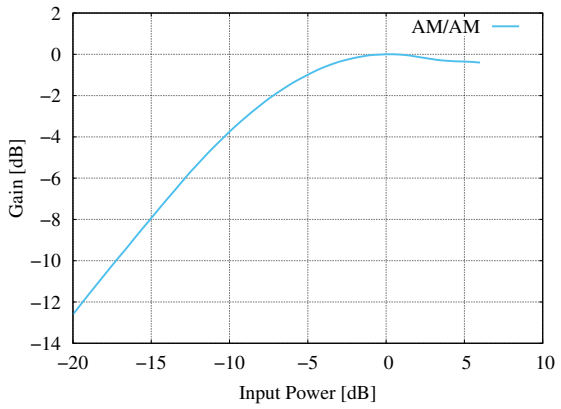

Fig. 3. AM/AM characteristic of the TWTA.

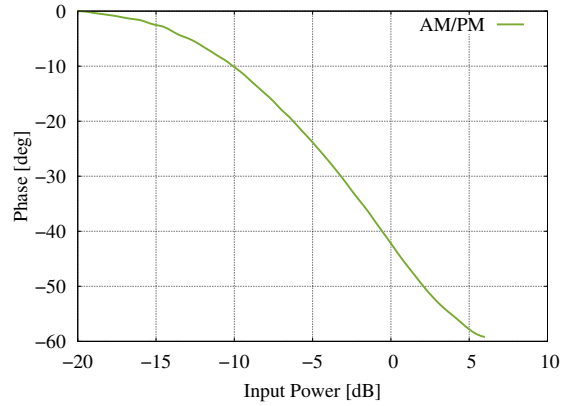

Fig. 4. AM/PM characteristic of the TWTA.

the receiver in [16] performing a closed-loop cancellation of telemetry and ranging signals from the received stream. Figure 5 shows the receiver block diagram.

Assuming an ideal lock and in the absence of nonlinear distortions, the ranging component is removed from the received signal by using a locally generated replica of the ranging signal. Mathematically,

$$y(t)r^*_{\text{RG}}(t-\hat{\tau}_{\text{RG}}) = x_{\text{TM}}(t) + w(t)r^*_{\text{RG}}(t-\hat{\tau}_{\text{RG}})\,, \quad (6)$$

being $r^*_{\text{RG}}(t)$ the ranging signal's complex conjugate locally generated using the estimated time delay $\hat{\tau}_{\text{RG}}$. It is easy to see that, being $r_{\text{RG}}(t)$ a phasor, the resultant process $w(t)r^*_{\text{RG}}(t-\hat{\tau}_{\text{RG}})$ is still white Gaussian, and $x_{\text{TM}}(t)$ is perfectly recovered as long as $\hat{\tau}_{\text{RG}} = \tau_{\text{RG}}$. The telemetry stream thus obtained is demodulated to extract data and then re-modulated to obtain the sequence of symbols. With it, we generate the complex conjugate $x^*_{\text{TM}}(t)$, necessary to sub-optimally cancel the telemetry

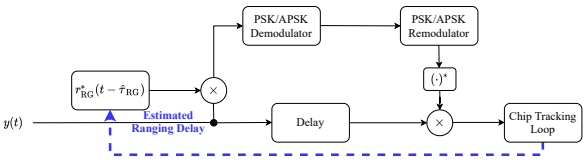

Fig. 5. Receiver block diagram.

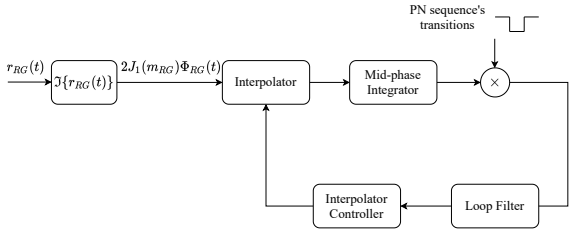

Fig. 6. Chip tracking loop block diagram.

component from the received signal. We can write

$$y(t)x^*_{\text{TM}}(t) = r_{\text{RG}}(t-\tau_{\text{RG}})|x_{\text{TM}}(t)|^2 + \mathcal{W}(t)\,, \quad (7)$$

where $\mathcal{W}(t) = x^*_{\text{TM}}(t)w(t)$ can be proved[1] to be a white process with power spectral density equal to N_0. Since $x_{\text{TM}}(t)$ is SRRC filtered, $|x_{\text{TM}}(t)|^2 \neq 1$, and thus perfect cancellation cannot be achieved. However, taking into account that $\mathbb{E}[|x_{\text{TM}}(t)|^2] = 1$, sub-optimal cancellation can be performed by averaging the samples of the telemetry signal's time-varying envelope, as shown later in Section IV.

Once recovered, the ranging sequence is input to the chip tracking loop (CTL), whose block diagram is depicted in Figure 6. Since the ranging chip sequence resembles a clock signal, we implement the CTL as a modified version of the data transition tracking loop (DTTL) [10], [18]. In this case, the mid-phase integrator operates according to an Integrate and Dump approach, integrating the PN sequence over a time interval T_c between two consecutive chips. Then, the output of the mid-phase integrator multiplies the PN transition sequence to adjust the sign of the error at the input of the loop filter. Finally, the estimated CTL timing $\hat{\tau}_{\text{RG}}$ is fed back to the local PN generator in Figure 5, thus closing the receiver loop.

Although the here-presented receiver is sub-optimal, we found it capable of performing well. Additionally, the receiver modular design allows (potentially) re-using the acquisition and synchronization chains adopted in a classical PSK/APSK demodulator (as the one in [14]) and in a CTL, thus using the same approach currently implemented for GMSK with PN ranging [3], [16]. In particular, since the GMSK can be seen as a quaternary modulation, we expect the QPSK synchronization and PN acquisition to work similarly. Differently, the classical synchronization could be subject to higher losses when dealing with higher-order PSK/APSK modulations. However, the high SNR (driven by the high bit rate), or the use of pilots as foreseen by standards[2], can compensate for the additional losses. In light of this, the remainder of this paper entirely focuses on the performance in tracking

[1]It is pointed out that the signal $x_{\text{TM}}(t)$ is actually a cyclostationary process, thus making $\mathcal{W}(t)$ cyclostationary as well. However, without loss of generality, in this paper we consider their stationary statistics by simply referring to the cyclic auto-correlation at null cyclic frequency [17].

[2]For instance, CCSDS 131.2 foresees the use of $\pi/2$-BPSK pilots [13], [14].

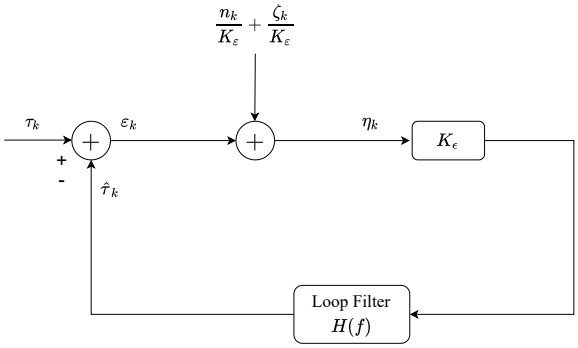

Fig. 7. Linearized CTL model.

conditions. The detailed study of the synchronization is left open for future implementation studies on this topic.

IV. Ranging Timing Jitter

In this section, we analyze the timing jitter of the receiver scheme presented in Section III.

We define $\mathcal{P}(t) = |x_{\text{TM}}(t)|^2 - 1$ as a zero-mean signal. Thus, Equation (7) can be re-written as

$$\begin{aligned} y(t)x^*_{\text{TM}}(t) =& r_{\text{RG}}(t-\tau_{\text{RG}}) + \mathcal{W}(t) + \\ & r_{\text{RG}}(t-\tau_{\text{RG}})\mathcal{P}(t)\,, \end{aligned} \tag{8}$$

where the last term can be understood as additional noise arising from the non-constant envelope of the considered modulation formats. To assess the effects generated by this new noise term, we analyze the output of the CTL. As Figure 6 shows, the CTL extracts the imaginary component of the ranging signal, which reads

$$\alpha\Phi_{\text{RG}}(t-\tau_{\text{RG}}) + \mathcal{N}(t) + \mathcal{D}(t)\,, \tag{9}$$

where $\mathcal{N}(t)$ is the imaginary component of the Gaussian noise, $\mathcal{D}(t) = \alpha\Phi_{\text{RG}}(t-\tau_{\text{RG}})\mathcal{P}(t)$, and[3] $\alpha \approx 2J_1(m_{\text{RG}})$. Thus, the ranging signal power at the CTL input is $P = \alpha^2/2$. Therefore, we define $n_k \triangleq \int_{kT_c}^{(k+1)T_c} \mathcal{N}(t)\,\mathrm{d}t$ and $\zeta_k \triangleq \int_{kT_c}^{(k+1)T_c} \mathcal{D}(t)\,\mathrm{d}t$, i.e., the output of the mid-phase integrator when $\mathcal{N}(t)$ and $\mathcal{D}(t)$ are the inputs, with auto-correlation $\mathcal{R}_n[k]$ and $\mathcal{R}_\zeta[k]$, respectively. While it is easy to see that $\mathcal{R}_n[k] = (N_0T_c/2)\delta_k$, a closed-form solution for $\mathcal{R}_\zeta[k]$ is not easy to obtain. However, as shown later, it can be numerically characterized.

At this stage, we are ready to derive a linearized model of the CTL, as reported in Figure 7, in which both the discretized noise terms at the k-th time (n_k and ζ_k) are added to the phase detector output ε_k. The loop error is defined as

$$\eta_k = \varepsilon_k + \frac{n_k}{K_\varepsilon} + \frac{\zeta_k}{K_\varepsilon}\,, \tag{10}$$

where $K_\varepsilon = 2\sqrt{2P}$ is the mid-phase integrator gain [10]. Therefore, considering that η_k is input to the loop filter having transfer function $H(f)$, the relation that describes the ranging timing jitter σ^2_τ reads

$$\sigma^2_\tau = T_c \int_0^{1/T_c} \left| \frac{K_\varepsilon H(f)}{1 + K_\varepsilon H(f)} \right|^2 S_\eta(f) df\,, \tag{11}$$

being $S_\eta(f)$ the power spectral density of the input η_k. Since the integrated loop bandwidth is usually very narrow w.r.t. the ranging signal rate, (11) can be rewritten as

$$\sigma^2_\tau \approx T_c \int_0^{1/T_c} \left| \frac{K_\varepsilon H(f)}{1 + K_\varepsilon H(f)} \right|^2 df\, S_\eta(0)\,. \tag{12}$$

Considering that the integral in (12) is the definition of the loop bandwidth B_L [19], and that the random variables n_k and ζ_k are uncorrelated, we can finally approximate the ranging timing jitter as

$$\sigma^2_\tau \approx \frac{2B_LT_c}{K^2_\varepsilon}\left[\sum_k \mathcal{R}_n[m] + \sum_k \mathcal{R}_\zeta[k]\right] \tag{13}$$

$$= \frac{2B_LT_c}{K^2_\varepsilon}\left[\frac{N_0T_c}{2} + \alpha^2T_c^2\sigma^2_\zeta\right] \tag{14}$$

$$= T_c^2\left(\frac{1}{8}\frac{N_0B_L}{P} + \frac{\sigma^2_\zeta B_LT_c}{2}\right)\,, \tag{15}$$

where, with an abuse of notation, it has been defined $\sum_k \mathcal{R}_\zeta[k] = \alpha^2T_c^2\sigma^2_\zeta$, explicitly reporting its dependence on the time and power factors T_c^2 and α^2.

Interestingly, ζ_k can be seen as an additional white noise process[4]. Namely, we observe that the first right-hand term in Equation (15) coincides with the theoretical PN ranging jitter [10] and decreases as P/N_0B_L grows. However, due to the non-constant envelope of the modulation, the second term appears, acting as an additional interference. Since this interference is proportional to B_L, the only way to reduce it is by narrowing the noise loop bandwidth, i.e., averaging the samples of the varying envelope.

The term σ^2_ζ, representing the normalized sum (with respect to $T_c^2\alpha^2$) of the coefficients of the auto-correlation function, depends on the modulation scheme, roll-off factor, and telemetry-symbol-rate to chip-rate ratio. Therefore, finding a closed-form solution can be cumbersome. However, as Section V will show, σ^2_ζ can be easily calculated through computer simulations, estimating the auto-correlation of the mid-phase integrator output when $\mathcal{D}(t)$ is given as input.

V. Numerical Results

In this section, we first present the performance of the designed telemetry ranging system from a physical layer perspective. Namely, we report the BER and timing jitter (derived through numerical simulations) in Subsection A. Then, using these results, in Subsection B, we analyze the performance of the proposed communication architecture

[3]Considering sine-shaped chip pulses, applying the Jacobi-Anger expansion we have $r_{\text{RG}}(t) \approx J_0(m_{\text{RG}}) + j2J_1(m_{\text{RG}})\Phi_{\text{RG}}(t)$ [16].

[4]Similar conclusion was found in [20], where the authors assumed ζ_k to be a white process, and derived an upper bound for σ^2_τ.

at a satellite system level, by taking as a reference the near-Earth SR mission GAIA and the still ongoing study of the European Space Agency GAIA-NIR.

A. Physical Layer Results

We simulate the transmission of a SRRC-filtered telemetry signal, PSK/APSK modulated (with order ranging from 4 to 64), having channel symbol rate $R = 1/T = 4.2$ Msymbol/s, and together with a PN ranging signal of rate $R_c = 1/T_c = 3$ Mchip/s. For the sake of simplicity, at the receiving end, we consider a CTL of the first order. However, the extension to higher-order loops, for better tracking effects as Doppler and Doppler rate, can be easily done employing standard design techniques [19]. Firstly, we carry out simulations under linear conditions with the AWGN channel. These serve as a benchmark for the nonlinear results later provided.

1. *Linear channel*

We first estimate σ_ζ^2 of (15) by characterizing the auto-correlation function $\mathcal{R}_\zeta[k]$. For the sake of clarity, Figure 8 shows the example for a QPSK-modulated telemetry stream, with roll-off 0.2: we derive the most significant components of the auto-correlation function, like the ones provided in the picture, via Monte Carlo simulations. Then, σ_ζ^2 is approximated as a sum of these elements. We repeat this approach for different modulation formats and roll-off factors and obtain the estimated values reported in Table I. Here, we can observe a common trend regardless of the modulation order: the higher the roll-off factor is, the smaller σ_ζ^2 becomes. In line with the expectations, higher roll-off factors correspond to a more constant envelope of the telemetry signal and, thus, lower power fluctuations. Additionally, by fixing the roll-off factor to 0.2, we analyze σ_ζ^2 when the telemetry-symbol-rate to chip-rate ratio, R/R_c, changes. The findings, presented in Figure 9, highlight an almost descending and linear behavior of σ_ζ^2 for increasing values of R/R_c for QPSK and 8-PSK, which results in a decrease of the ranging timing jitter floor. In fact, by increasing the number of symbols per chip input to the CTL, there is a better averaging of the samples, thus reducing the telemetry power fluctuations. Whereas, we cannot draw the same conclusion for 16-, 32-, and 64-APSK for which there is no sharp reduction of σ_ζ^2 as R/R_c increases. Additionally, these curves do not express a linear behavior.

Now, we analyze the ranging jitter in the ideal condition of perfectly demodulated telemetry symbols. In this way, we assess how the SRRC filtering impacts the timing recovery regardless of erroneous demodulation events. To do so, we implement and simulate a genie-aided receiver provided with the correct sequence of symbols $\{a_k\}$. We then evaluate the timing jitter σ_τ^2, normalized to T_c^2, via Monte Carlo simulations, as a function of the signal-to-noise ratio P/N_0B_L and for different values of B_L. Figure 10 and 11 present the simulation results for SRRC filtered (roll-off = 0.2) QPSK and 64-APSK modulations

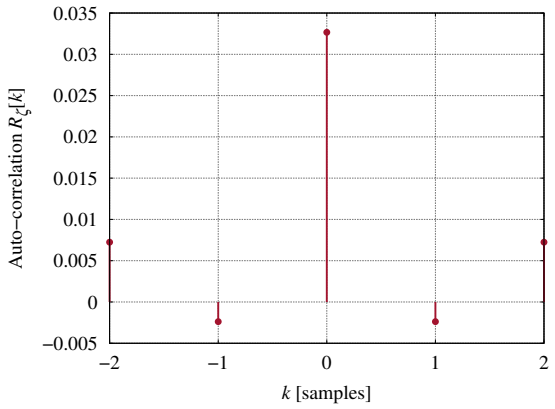

Fig. 8. Discrete-time auto-correlation function $\mathcal{R}_\zeta[m]$ for a QPSK-modulated telemetry stream (roll-off = 0.2).

TABLE I
σ_ζ^2 approximated values (in [dB]) for different modulations and roll-off factors.

Roll-off	QPSK	8-PSK	16-APSK	32-APSK	64-APSK
0.2	-13.8	-13.9	-12.9	-12.4	-12.8
0.25	-13.9	-14.1	-13.0	-12.4	-12.8
0.3	-14.1	-14.3	-13.2	-12.6	-13.0
0.35	-14.4	-14.6	-13.3	-12.7	-13.1

with the genie-aided receiver. For comparison the figures include also the curves derived by means of (15) (by using the estimated σ_ζ^2 in Table I) and the jitter of the PN ranging with GMSK-modulated telemetry signal. As foretold, the jitter has a floor that decreases with B_L, and thus the performance gets closer to the GMSK jitter. In particular, B_L equal to 150 Hz provides almost an ideal performance without limiting the timing synchronization dynamic. Additionally, the closed formula expression well predicts σ_τ^2.

Finally, we evaluate the end-to-end performance of the receiver scheme of Figure 5 from the telemetry and ranging points of view by simulating the complete communication chain for all SRRC filtered PSK/APSK

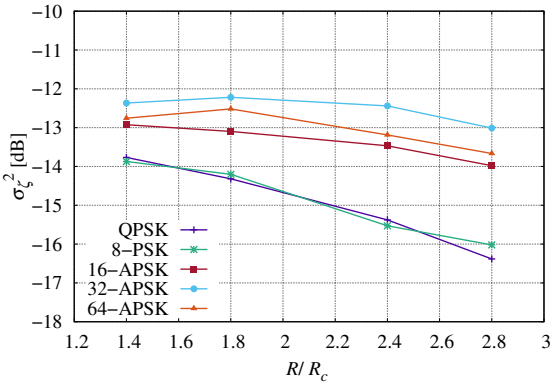

Fig. 9. σ_ζ^2 as function of R/R_c for different modulation schemes and roll-off factor 0.2.

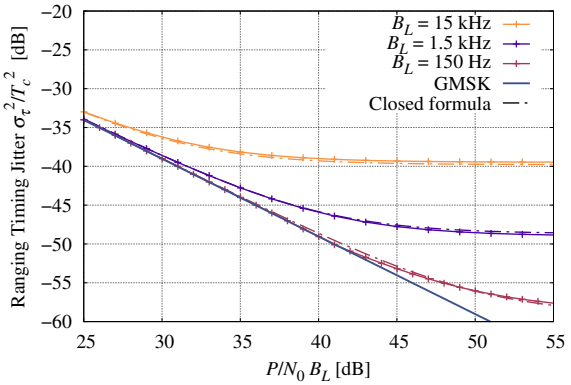

Fig. 10. Impact of SRRC-filtered QPSK modulation (roll-off = 0.2) on ranging timing jitter, computed by using a genie-aided receiver.

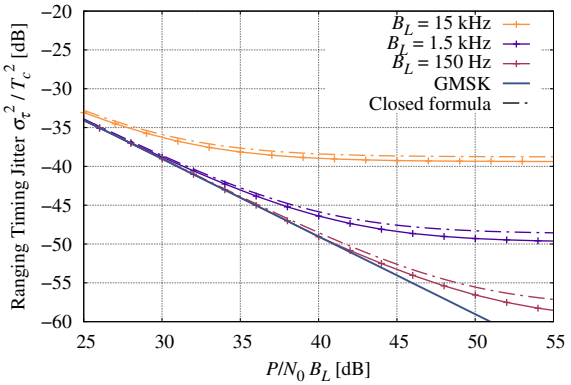

Fig. 11. Impact of SRRC-filtered 64-APSK modulation (roll-off = 0.2) on ranging timing jitter, computed by using a genie-aided receiver.

modulations. Figures 12, 13, 14 and 15 present the ranging timing jitter as a function of P/N_0B_L and the telemetry's BER versus E_b/N_0 (being E_b the energy per bit). For comparison, the BER figures show also the theoretical curve in AWGN and in absence of ranging. Figures 12 and 14, showing timing jitter performance, reveal the same trend for the modulation sets. Despite an initial deviation (more pronounced as the modulation order grows), the simulated ranging jitter curves converge to the genie-aided one. Moreover, although the telemetry and ranging performances are inherently intertwined, the worsened jitter performance for low values of P/N_0B_L, with respect to ideal cancellation, is not reflected in the BER. In fact, the end-to-end BER is comparable to the theoretical one. In light of this, one could use channel coding (e.g., the serially concatenated convolutional codes foreseen by CCSDS 131.2 [13]) and obtain the performance results found in [14] without a significant implementation loss.

2. *Nonlinear channel*

To consider a more realistic scenario that includes power amplification, we re-run the simulations under nonlinear conditions, with the channel model of Figure 2,

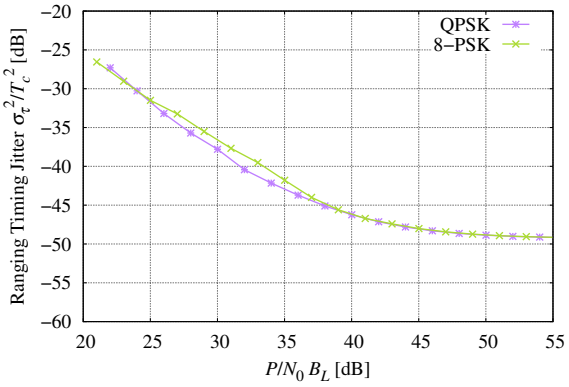

Fig. 12. AWGN end-to-end ranging timing jitter for QPSK and 8-PSK modulations ($B_L = 1.5$ kHz, roll-off = 0.2).

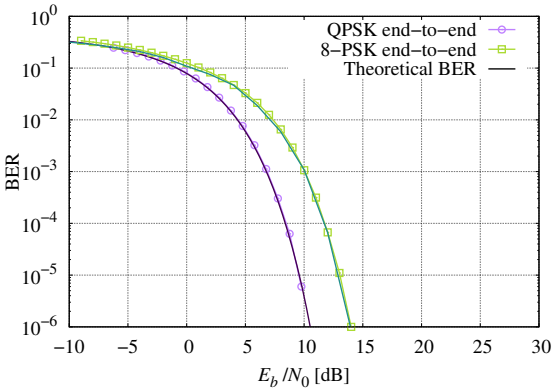

Fig. 13. AWGN end-to-end telemetry BER for 16-APSK, 32-APSK, and 64-APSK modulations ($B_L = 1.5$ kHz, roll-off = 0.2).

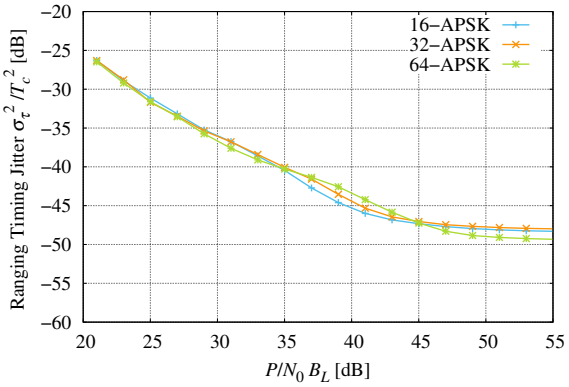

Fig. 14. AWGN end-to-end ranging timing jitter for 16-APSK, 32-APSK, and 64-APSK modulations ($B_L = 1.5$ kHz, roll-off = 0.2).

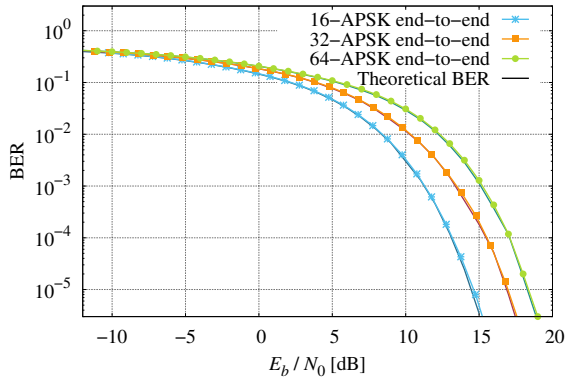

Fig. 15. AWGN end-to-end telemetry BER for 16-APSK, 32-APSK, and 64-APSK modulations ($B_L = 1.5$ kHz, roll-off = 0.2).

TABLE II

IBO and (corresponding) OBO values adopted for PSK/APSK modulations.

Modulation	OBO [dB]	IBO [dB]
QPSK	0.33	0
8-PSK	0.31	0
16-APSK	2.02	6
32-APSK	4.34	10
64-APSK	7.23	14

using the input and (corresponding) output back-off (IBO and OBO) values reported in Table II.

First, we analyze the occupied bandwidth, as 99-percent of the signal power, of GMSK (BT [5] $= 0.25$), PSK and APSK-modulated telemetry stream with different ranging modulation indexes. For a fair comparison, we consider a GMSK signal having a bit rate equal to the QPSK-modulated telemetry stream. Instead, we compare the other modulations using the same channel symbol rate.

Trivially, the spectral occupancy changes as a function of the ranging modulation index m_{RG}. As shown in Table III, the higher m_{RG} is, the more the spectrum broaden. This effect can be seen very well in Figure 16, that provides as example the spectra of 8PSK at the output of the RF filter, for different values of m_{RG}. Interestingly, despite the spectral regrowth caused by power amplification, the PSK/APSK scheme has an occupied bandwidth that is comparable to the one of the GMSK scheme.

Next, we simulate the end-to-end communication system. As for the linear case, we present results for QPSK and 64-APSK modulations, for which the ranging timing jitter is reported in Figures 17 and 18, respectively. The figures show both linear and nonlinear performance, revealing a gap of about 2 dB between the two due to distortions caused by the power amplification and the filtering process.

Finally, for assessing the telemetry performance, we analyze the BER degradation due to the presence of ranging. Figures 19 and 20 show an example for QPSK and

[5] BT is the normalized filter bandwidth

TABLE III

Occupied bandwidth for PSK and APSK (SRRC filtered with roll-off 0.35) and GMSK, over the nonlinear channel, as a function of the ranging modulation index m_{RG}.

m_{RG}	PSK	APSK	GMSK
0.111	7.4 MHz	7.1 MHz	7.22 MHz
0.222	7.6 MHz	7.4 MHz	7.31 MHz
0.444	8.4 MHz	8.1 MHz	7.72 MHz
0.666	8.7 MHz	8.7 MHz	8.23 MHz

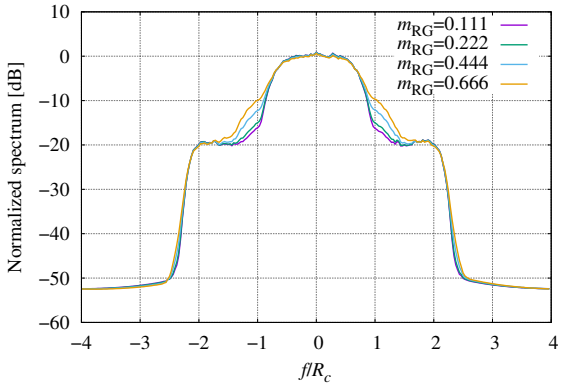

Fig. 16. Normalized spectra for 8PSK, over the nonlinear channel, as a function of the ranging modulation index m_{RG}.

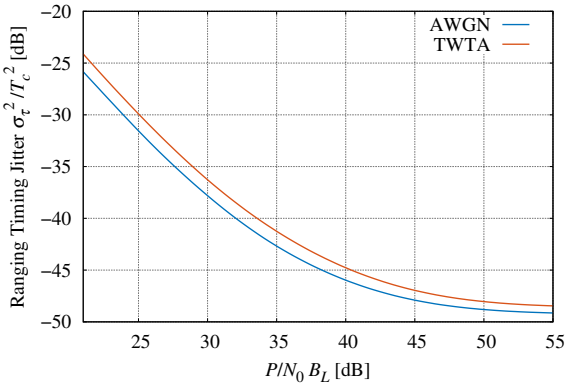

Fig. 17. End-to-end ranging timing jitter for QPSK modulation under nonlinear conditions ($B_L = 1.5$ kHz).

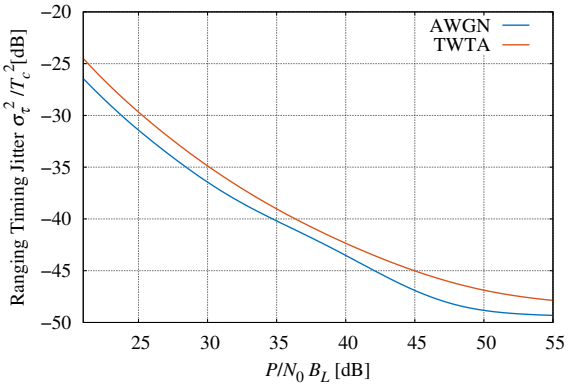

Fig. 18. End-to-end ranging timing jitter for 64-APSK modulation under nonlinear conditions ($B_L = 1.5$ kHz).

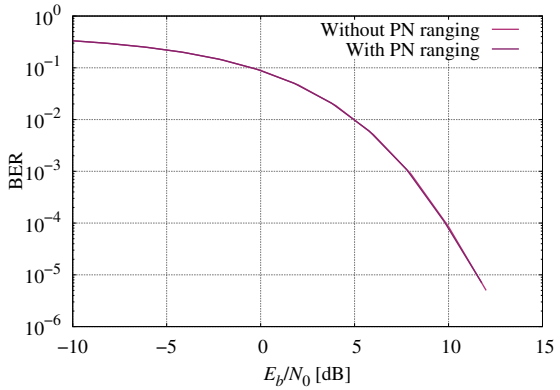

Fig. 19. Uncoded BER for QPSK on nonlinear channel with and without ranging signal (roll-off = 0.2).

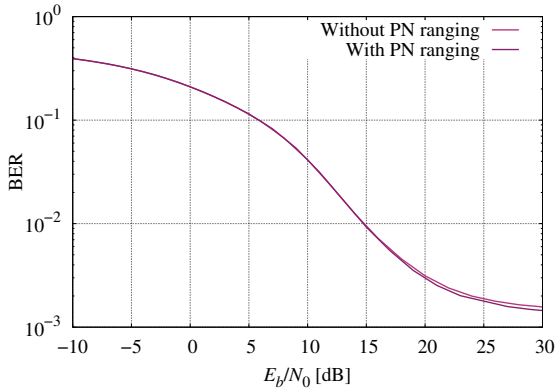

Fig. 20. Uncoded BER for 64-APSK on nonlinear channel with and without ranging signal (roll-off = 0.2).

64-APSK modulation, respectively. The obtained results imply no additional losses with respect to a scenario free of the ranging signal.

B. System Analysis Results

In this section, we adopt the results of the physical layer simulations for analyzing the performance of two cases of study: GAIA and GAIA-NIR. GAIA [22] is an ESA mission launched in 2013 that achieved 8.7 Mbps in X-Band using a GMSK signal. GAIA-NIR, instead, is an ongoing ESA study that could improve the data return by using a higher equivalent isotropically radiated power (EIRP). Both mission scenarios need to maximize the achievable telemetry bit rate, while keeping a ranging accuracy below 5 meters. Consequently, this section aims to prove the gain in the data rate of the here-proposed communication architecture for these two mission scenarios with respect to the use of the state-of-the-art GMSK and PN ranging scheme.

To pursue our goal, we carry out a link budget analysis, for which we choose the Cebreros site [23] as the receiver station. For modulation and coding formats (modcods), we consider the 27 modcods provided in CCSDS 131.2 ([13], [14]), which foresees PSK/APSK

TABLE IV
GAIA/GAIA-NIR link budgets.

	GAIA		GAIA-NIR	
	Best	Worst	Best	Worst
Frequency [MHz]	8500	8500	8500	8500
EIRP [dB]	34	34	45	45
Sat. altitude [km]	1368000	1760000	1368000	1760000
Elevation angle [deg]	50	10	50	10
Slant Range [km]	1369486	1765259	1369486	1765259
Path Loss [dB]	234	236	234	236
Atmospheric losses [dB]	0.27	1.04	0.27	1.04
G/T [dBK]	53.1	50.2	53.1	50.2
Rec. SNR [dBHz]	81.7	75.8	92.7	86.8
Margin [dB]	3	3	3	3
Modcod	13	7	25	17
E_b/N_0 [dB]	4.45	2.41	10.07	7.58
Demodulation losses [dB]	2.40	0.95	5.27	3.44
Nonlinear losses [dB]	2	2	2	2
R_b [Mbps]	15.2	8.8	27.4	18.9
P/N_0B_L [dB]	39.7	33.9	50.8	44.9
Timing Jitter $\widetilde{\sigma}_\tau^2$ [dB]	-44.27	-39,92	-46.36	-45.7
Jitter [m]	0.61	1.00	0.48	0.52

modulations as those considered in this paper, with different coding rates. Starting from the satellite EIRP and the best and worst case satellite altitude, we select the modcod that maximizes the bit rate, while complying with the 10 MHz bandwidth limitation [4]. Then, we assess the ranging jitter (in meters) when using a CTL bandwidth B_L of 1.5 kHz, which does not limit the timing tracking in presence of Doppler[6].

Table IV summarizes the findings of the link budget. According to this, GAIA, in the best case, would employ the modcod 13 (16-APSK), leading to a bit rate of 15.2 Mbps. In the worst case, instead, it can achieve up to 8.8 Mbps by means of modcod 7 (8-PSK). GAIA-NIR, on its own, can reach a bit rate of 27.4 Mbps by means of modcod 25 (64-APSK), and 18.9 Mbps by means of modcod 17 (16-APSK). In all cases, the ranging jitter was below 1 meter. Consequently, the results in Table IV highlight how the proposed system overcomes the current bit rate limit while achieving the required ranging performance.

VI. Conclusions

In this paper, we investigated the possibility of combining the PN ranging with high-order, spectrally-efficient PSK/APSK modulations. At the receiver side, we designed, implemented, and simulated a receiver scheme for simultaneous demodulation of high-order telemetry symbols and tracking the received ranging sequence for orbit determination. The obtained results show that it is possible to achieve ranging performance comparable to current state-of-the-art receiver architecture by simply

[6]For instance GAIA and GAIA-NIR could adopt a loop bandwidth as low as 1 mHz.

lowering the noise loop bandwidth B_L. Furthermore, the use of such modulations in telemetry-ranging systems enables a data rate way higher than 10 Mbps.

REFERENCES

[1] CCSDS 414.1-B-2, *Pseudo-Noise PN Ranging Systems*, Feb. 2014, Available at http://public.ccsds.org/.

[2] J. B. Berner, P. W. Kinma, and J. M. Layland, "Regenerative pseudo-noise ranging for deep space applications," in *ESA 3rd Workshop on Tracking, Telemetry and Command Systems for Space Applications*, Noordwijk, The Netherlands, Oct. 2001.

[3] M. Mascarello, G. Sessler, E. Vassallo, G. R. Iglesias, K. Kewin, M. Montagna, and L. Manso, "The Solar Orbiter X-Band TT&C New Features: GMSK with PN Regenerative Ranging and DDOR Semaphores Implementation," in *2019 8th International Workshop on Tracking, Telemetry and Command Systems for Space Applications (TTC)*, Sep. 2019, pp. 1–6.

[4] Space Frequency Coordination Group, *Use of the 8450-8500 MHz Band for Space Research, Category A*, Feb. 1998, Available at https://sfcgonline.org/.

[5] ECSS-E-ST-50-05C, *Radio frequency and modulation*, Oct. 2011, Available at https://ecss.nl/.

[6] O. Montenbruck and E. Gill, *Satellite orbits*, 1st ed. Springer Verlag, Heidelberg, 2000.

[7] S. Hackel, P. Steigenberger, U. Hugentobler, M. Uhlemann, and O. Montenbruck, "Galileo orbit determination using combined GNSS and SLR observations," *GPS solutions*, vol. 19, no. 1, pp. 15–25, Apr. 2015.

[8] Jet Propulsion Laboratory, California Institute of Technology, "DSN telecommunications link design handbook," JPL, Tech. Rep., 2010.

[9] ECSS-E-ST-50-02C, *Ranging and Doppler Tracking*, Jul. 2008, Available at https://ecss.nl/.

[10] CCSDS 414.0-G-2, *Pseudo-Noise PN Ranging Systems*, Feb. 2014, Available at http://public.ccsds.org/.

[11] I. Di Stefano, L. Iess, P. Cappuccio, and M. Di Benedetto, "Orbit determination during JUICE cruise phase to test fundamental physics," *43rd COSPAR Scientific Assembly.*, vol. 43, p. 2118, Jan. 2021.

[12] P. Cappuccio, V. Notaro, L. Iess, S. Asmar, J. Border, S. Ciarcia Sr, A. Di Ruscio, E. Montagnon, J. De Vicente, M. Mercolino *et al.*, "First results from cruise tests of the mercury orbiter radio science experiment (MORE) of ESA's BepiColombo mission," *AGUFM*, vol. 2019, Dec. 2019.

[13] CCSDS 131.2-B-1, *Flexible advanced coding and modulation scheme for high rate telemetry applications*, Mar. 2012, Available at http://public.ccsds.org/.

[14] CCSDS 130.11-G-1, *SCCC—Summary of definition and performance*, Apr. 2019, Available at http://public.ccsds.org/.

[15] CCSDS 401.0-B-31, *Radio Frequency and modulation systems - Part 1 Earth Stations and Spacecrafts*, Feb. 2020, Available at http://public.ccsds.org/.

[16] CCSDS 413.1-G-2, *Simultaneous transmission of GMSK telemetry and PN Ranging*, Nov. 2021, Available at http://public.ccsds.org/.

[17] A. Papoulis, *Probability, Random Variables and Stochastic Processes*. New York, NY: McGraw-Hill, 1991.

[18] Jet Propulsion Laboratory, California Institute of Technology, "Autonomous software-defined radio receivers for deep space applications," JPL, Tech. Rep., 2006.

[19] F. M. Gardner, *Phaselock techniques*, 3rd ed. John Wiley & Sons, 2005.

[20] B. Ripani, A. Modenini, R. Garello, G. M. Capez, and G. Montorsi, "On the use of PN Ranging with High-rate Spectrally-efficient Modulations," in *Proc. Intern. Conf. on Space Operations (SpaceOps)*, Virtual conference, May 2021.

[21] R. Xue, T. Wang, and H. Tang, "A novel chip pulse employed by ranging code based on simultaneous transmitting cpm modulation and pn ranging in inter-satellite links of gnss," *IEEE Access*, vol. 8, pp. 132 860–132 870, 2020.

[22] European Space Agency, "GAIA flight model payload data handling unit delivered and integrated," Available at https://sci.esa.int/web/gaia/.

[23] European Space Operations Centre ESOC, "ESA Tracking Stations (ESTRACK) Facilities Manual," 2008, DOPS-ESTR-OPS-MAN-1001-OPS-ONN.

Barbara Ripani (S22) received the Bachelor Degree from Università Politecnica delle Marche in Biomedical Engineering in 2018, and the Master Degree from Politecnico di Torino in Communications and Computer Networks Engineering in 2021. She carried out her Master Degree thesis at the European Space Research Technology Center (ESTEC) on the coupling of Pseudo-Noise ranging with high-order modulated telemetry signals, followed by a postgraduate traineeship. During this period she gained experience in designing TT&C and PDT subsystems for space missions in early phases, supported satellite assembly, integration, and testing activities, and got involved in standardization activities. She is currently working toward the Ph.D., which started in September 2021 at Politecnico di Torino, under the supervision of Prof. Guido Montorsi. Her research topic focuses on synchronization challenges in time selective channels. In January 2022, she became a student member of IEEE, AESS, and ComSoc societies.

Andrea Modenini was born in Parma, Italy, on September 15, 1986. He received the MSc in Telecommunications Engineering (cum laude) on December 13, 2010 and the Ph.D. in January 2014 from the University of Parma.

Since March 2015, he is at the European Space Agency (ESA), ESTEC site (Noordwijk, The Netherlands), currently working as TT&C Communications Systems Engineer, supporting ESA Earth Observation and Scientific satellite missions, research and development for TT&C units, techniques, and the design of the command and control (C2) for unmanned aerial vehicles (UAVs). He is also supporting the education in the field of TT&C as tutor of ESA trainees. Finally, he is involved in several standardization activities for satellite telecommunications in the framework of ECSS, SFCG, and CCSDS. For the latter, he is Chair of the Coding & Synchronization working group.

In 2014 he was postdoctoral researcher at the Dipartimento di Ingegneria dell'Informazione (DII) in Professor Giulio Colavolpe Research Group. In the spring 2012 he was a visiting PhD student in the group of Prof. Fredrik Rusek of the Elektro- och informationsteknik of the University of Lund, Sweden, for research on channel shortening detection for spectrally efficient modulations.

In June 2014 he won the award issued by GTTI for the best PhD thesis discussed in Italy.

He served also as a Technical Program Committee (TPC) member for ASMS/SPSC 2012, Baiona, Spain, and ASMS/SPSC 2014, Livorno, Italy.

Guido Montorsi (F19) Received the Laurea in Ingegneria Elettronica in 1990 from Politecnico di Torino. In 1992 he spent the year as visiting scholar in the Department of Electrical at the Rensselaer Polytechnic Institute, Troy, NY. In 1994 he received the Ph.D. degree in telecommunications from the Dipartimento di Elettronica of Politecnico di Torino. In December 1997 he became assistant professor at the Politecnico di Torino. From July 2001 to July 2002 he spent one year at Sequoia Communications, a company developing baseband algorithms for 3G wireless receivers. In 2003 he became senior member of IEEE and associate professor at Politecnico di Torino. In 2013 he became full professor at Politecnico di Torino. Guido Montorsi is author of more the one hundred papers on international journals and conferences. He served as TPC member in several IEEE conferences. His research interests are in the area of channel coding, particularly on the analysis and design of concatenated coding and modulation schemes and study of iterative strategies for advanced receivers. He is IEEE fellow from 2019.